Voigt Exceptional Points in an Anisotropic ZnO-Based Planar Microcavity: Square-Root Topology, Polarization Vortices, and Circularity

Steffen Richter,[1,2,*] Heinrich-Gregor Zirnstein,[3] Jesús Zúñiga-Pérez,[4] Evgeny Krüger,[1] Christiane Deparis,[4] Lukas Trefflich,[1] Chris Sturm,[1] Bernd Rosenow,[3] Marius Grundmann,[1] and Rüdiger Schmidt-Grund[1,5]

[1]*Universität Leipzig, Felix-Bloch-Institut für Festkörperphysik, Linnéstraße 5, 04103 Leipzig, Germany*
[2]*ELI Beamlines/Fyzikální ústav AV ČR, Za Radnicí 835, 25241 Dolní Břežany, Czech Republic*
[3]*Universität Leipzig, Institut für Theoretische Physik, Brüderstraße 16, 04103 Leipzig, Germany*
[4]*Université Côte d'Azur, CRHEA-CNRS, rue Bernard Grégory, 06560 Valbonne, France*
[5]*Technische Universität Ilmenau, Institut für Physik, Weimarer Straße 32, 98693 Ilmenau, Germany*

(Received 28 October 2018; published 26 November 2019)

Voigt points represent propagation directions in anisotropic crystals along which optical modes degenerate, leading to a single circularly polarized eigenmode. They are a particular class of exceptional points. Here, we report the fabrication and characterization of a dielectric, anisotropic optical microcavity based on nonpolar ZnO that implements a non-Hermitian system and mimics the behavior of Voigt points in natural crystals. We prove the exceptional-point nature by monitoring the complex-square-root topology of the mode eigenenergies (real and imaginary parts) around the Voigt points. Polarization state analysis shows that these artificially engineered Voigt points behave as vortex cores for the linear polarization and sustain chiral modes. Our findings apply to any planar microcavity with broken cylindrical symmetry and, thus, pave the way for exploiting exceptional points in widespread optoelectronic devices such as vertical cavity surface emitting lasers and resonant cavity light emitting diodes.

DOI: 10.1103/PhysRevLett.123.227401

The search for topologically nontrivial, photonic systems [1–5] has raised interest in exceptional points (EPs), i.e., non-Hermitian degeneracies of complex-valued eigenenergies that represent topological charges [6–14]. In optical systems, such branching points have been reported in the eigenmodes of ring resonators, photonic crystals, and waveguides [14–17]. Voigt waves [18,19] are an early example of EPs that are associated with the propagation of circularly polarized light in a three-dimensional crystal. Here, a key requirement is optical biaxiality, which can also be established by confining a uniaxial material in two-dimensional planar microcavities [20] that are essential building blocks in optoelectronic technology (e.g., vertical cavity surface emitting lasers).

In anisotropic crystals, optical mode degeneracies are connected to different types of singularities, depending on whether the material is transparent or absorptive: In transparent biaxial media, classic optic axes are diabolical points in momentum space, known as Dirac or Hamilton points [21]. The mode dispersion displays a conical intersection that, in turn, leads to conical refraction [22–24]. If biaxial materials are absorbing, classic optic axes split into pairs of singular optic axes [19,25]. For propagation along them, the eigenspace of optical modes becomes one dimensional, allowing only either right or left circularly polarized wave fronts to travel without change of polarization. Only for these directions, both real (refractive index) and imaginary (extinction coefficient) parts of the propagation constants degenerate simultaneously. Thus, singular optic axes are EPs in momentum space. Analogously to the diabolical Hamilton points, we term them Voigt points, going back to their discovery by Woldemar Voigt in 1902 [26,27]. With circularly polarized eigenmodes, Voigt points are an elegant demonstration of chirality which is a fingerprint of EPs [12,28,29].

Natural occurrence of Voigt points requires polarization-dependent absorption or gain, which are intrinsic material properties and hard to modify. To overcome this limitation, we consider a conventional planar microcavity and count on the dissipation caused by photon loss rather than material absorption. The design degrees of freedom (e.g., mirror reflectivities, cavity and mirrors' central wavelengths, etc.) allow a planar microcavity of fully transparent, anisotropic materials to display Voigt points readily accessible within the vacuum light cone [20]. In this Letter, we report the fabrication and optical characterization of such a system based on *m*-plane oriented ZnO. We have measured reflected Stokes vector spectra for all in-plane momenta [$\vec{k}_{\parallel}$, Fig. 1(a)] of the radiative cavity photon modes, and determined their complex-energy dispersion by modeling with an effective, non-Hermitian Hamiltonian. While $\vec{k}_{\parallel} = (k_x, k_y)$ represents an easily tunable parameter, defined by the incident light direction, polarization analysis is the key to reliable mode tracking to prove the complex-square-root topology of the mode-energy surface and,

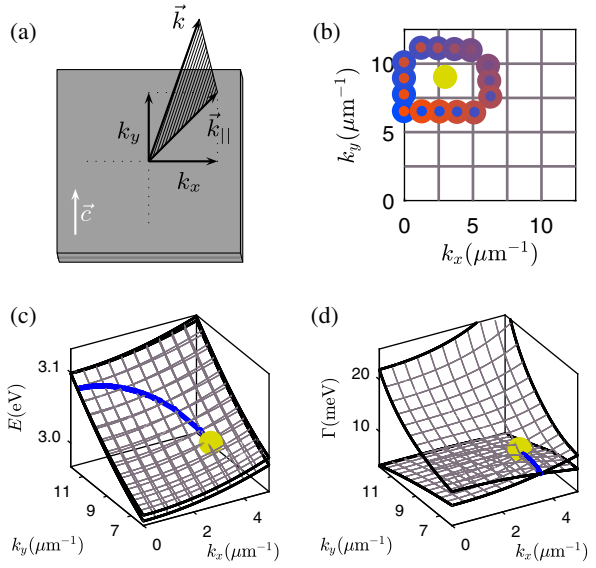

FIG. 1. (a) Sketch of the planar microcavity and coordinates of the in-plane wave vector $\vec{k}_{\parallel}$ related to the detected light. The material's optic axis ($\vec{c}$) is aligned with the y direction. (b) Schematic position of one Voigt point in the first $\vec{k}_{\parallel}$ quadrant (yellow dot), and path for encirclement (blue-to-red dots, cf. Fig. 4). (c),(d) Schematic shape of the complex-energy surface of the modes near this Voigt point (yellow sphere), illustrating the complex-square-root topology. Blue lines mark trajectories of degenerate energy $E_{1,2}$ and broadening $\Gamma_{1,2}$ which overlap only at Voigt points.

hence, the presence of EPs. The effective model describes how the latter emerge from a diabolical point and explains mode-interference effects that go beyond purely Lorentzian resonance peaks. We also present linear-polarization vortices around Voigt points and their correlation with circular polarization.

Theoretical considerations.—Light may interfere constructively in a microcavity if its wavelength is commensurable with the effective optical thickness of the cavity layer, giving rise to standing waves (eigenmodes). First, we consider a hypothetical anisotropic microcavity without losses. The two polarization-dependent resonance energies of a cavity mode are given by the eigenvalues of a real-valued, Hermitian 2×2 Hamiltonian $\hat{H}_0$

$$\hat{H}_0 = E_0\hat{1} + A\hat{\sigma}_x + B\hat{\sigma}_z, \tag{1}$$

where E_0 is the mean mode energy, A expresses polarization mixing due to the anisotropy of the cavity material [if k_x, $k_y \neq 0$, cf. Fig. 1(a)] and B reflects the energetic mode splitting due to different, polarization-dependent dispersions. $\hat{1}$ and $\hat{\sigma}_{x,z}$ denote the unit matrix and Pauli spin matrices, respectively. Since the optical thickness of the cavity depends on the propagation angle, the Hamiltonian and its coefficients are functions of the in-plane wave vector $\vec{k}_{\parallel}$. Parallel to the material's optic axis ($k_x = 0$), the modes are purely TE and TM polarized ($A = 0$). For our cavity configuration, the mode energies become degenerate at $k_y = \pm k_y^0$ [20]. These are two diabolical points which occur at opposite in-plane momenta due to the orthorhombic symmetry of the microcavity. Near them, a linear expansion gives $A \propto k_x$, $B \propto |k_y| - |k_y^0|$, and $E_0 \propto |k_y|$. Thus, they are type-II Dirac points [30].

A real microcavity is leaky and the cavity modes couple to the outside. Using the Mahaux-Weidenmüller formula [31], this can be described by a 2×4 matrix $\hat{W}$ which couples four incoming field components (TE and TM polarization on the top and bottom sides of the microcavity) to the two modes. Effectively, the modes turn into resonances with complex-valued eigenenergies $\tilde{E}_{1,2} = E_{1,2} - i\Gamma_{1,2}$ whose imaginary part describes the exponential decay of the electromagnetic field of a mode. The mode energies are the eigenvalues of the non-Hermitian Hamiltonian $\hat{H} = \hat{H}_0 - i\hat{W}\hat{W}^{\dagger}$. For a microcavity that is symmetric under reflection along the z axis, we can decompose $\hat{W} = (\hat{w}\,\hat{w})$ with a 2×2 matrix $\hat{w}$, where

$$\hat{w} = \sqrt{\frac{1}{2}}\begin{pmatrix} \sqrt{\Gamma_0 - C} & 0 \\ 0 & \sqrt{\Gamma_0 + C} \end{pmatrix}\begin{pmatrix} u & -v^* \\ v & u^* \end{pmatrix}, \tag{2}$$

with real-valued parameters Γ_0, C with $\Gamma_0 \geq |C|$, and u, $v \in \mathbb{C}$ with $|u|^2 + |v|^2 = 1$. Γ_0 is mean mode broadening (photon loss) and C indicates the polarization dependence of the loss. To lowest order near the mode degeneracies, Γ_0 and C are constant. The transformation matrix described by u and v allows adjusting the polarization (see below). Consequently, it holds

$$\hat{H} = \hat{H}_0 - i\Gamma_0\hat{1} + iC\hat{\sigma}_z. \tag{3}$$

The eigenvalues are

$$\tilde{E}_{1,2} = E_0 - i\Gamma_0 \pm \sqrt{A^2 + (B + iC)^2}. \tag{4}$$

They coincide, $\tilde{E}_1 = \tilde{E}_2$, when $B = 0$ and $|C| = |A|$. In linear approximation near a diabolical point of $\hat{H}_0$, we find this fulfilled at $k_x = k_x^0 \propto \pm C$, $k_y = k_y^0$. These locations are EPs where the Hamiltonian $\hat{H}$ has degenerate eigenvalues, but cannot be diagonalized. Thus, a polarization-dependent loss $C \neq 0$, due to the optical anisotropy of the microcavity, will cause each diabolical point to split into a pair of EPs. They are connected by a curve of coinciding real parts, $E_1 = E_2$, characterized by $B = 0$ and $|A| < |C|$ [cf. blue line in Fig. 1(c)]. The pairs of EPs are connected by a curve with coinciding imaginary part, $\Gamma_1 = \Gamma_2$, where $B = 0$ and $|A| > |C|$ [blue line in Fig. 1(d)]. The characteristic feature of an EP is the square-root topology of the complex

eigenvalue surface [6,32]: When varying the wave vector $\vec{k}_\parallel$ in order to encircle an EP once, continuously following the first mode $\tilde{E}_1(\vec{k}_\parallel)$ will end up in the second mode $\tilde{E}_2$ when the loop returns to its starting point.

The link between the effective non-Hermitian Hamiltonian (3) and experimentally measured optical spectra is provided by the Mahaux-Weidenmüller formula [31]. For a microcavity that is symmetric under reflection along the z axis, the reflection Jones matrix is given by

$$\hat{J}(E) = \hat{1} - 2i\hat{w}^\dagger(E\hat{1} - \hat{H})^{-1}\hat{w}. \tag{5}$$

In the experiment, we measured the energy-resolved Stokes vector when unpolarized light was reflected from the microcavity. From Eq. (5), we can directly compute the Müller matrix as a function of photon energy E. Its first column corresponds to the Stokes vector from the experiment. Strictly speaking, the above form of the Jones matrix requires a specific choice of the polarization basis for the incoming light. But we can ignore this in our case since we illuminate the microcavity with completely unpolarized light. The Hamiltonian Eq. (3), depending on the real-valued parameters A, B, C, E_0, Γ_0, is the most general way to express a 2×2 matrix up to a unitary basis change. A complementary parametrization of the coupling matrix $\hat{w}$ by parameters u and v [Eq. (2)] controls the polarization of the outgoing light. See, also, Supplemental Material (SM) [33].

Experimental approach.—We have fabricated an anisotropic ZnO-based planar microcavity: First, a 16× ZnO/$Mg_{0.29}Zn_{0.71}$ O distributed Bragg reflector (DBR) and the ZnO cavity layer have been grown on m-plane oriented ZnO substrate by molecular-beam epitaxy [38]. The optical thickness of the cavity layer corresponds to 9/8 of the central wavelength of the DBR (≈400 nm), as previous numerical computations indicated this detuning well suitable for the observation of well-separated Voigt points [20,39]. All ZnO and $Mg_{0.29}Zn_{0.71}$ O layers are m-plane oriented and reveal interface roughnesses below 1 nm [38]. The top DBR was prepared nonepitaxially by pulsed laser deposition and consists of six pairs Al_2O_3 and Y-stabilized ZrO_2, all layers being optically isotropic [40]. While the top and bottom DBR are made from different materials, we have matched their reflectivities. The microcavity can be regarded as approximately mirror symmetric along the vertical axis. All materials are transparent in the energy range of the cavity photon modes (3 eV).

We performed polarization-resolved reflection experiments depending on the angle of incidence θ (10°–75° from the surface normal) and sample azimuth angle ϕ (0°–360°). Almost 700 configurations (θ, ϕ) were used to map the momentum space of the radiative cavity modes; see Fig. 3. Unpolarized white light from a Xe lamp was reflected off the sample and the Stokes vector $\vec{S} = (S_0, S_1, S_2, S_3)$ obtained [41]. S_0 represents unpolarized reflectance. S_1, S_2, and S_3 are the intensity I differences between the light linearly polarized parallel to x and y, linearly polarized +45° and −45° vs x, and right- and left-circularly polarized, respectively. For each configuration (θ, ϕ), the four Stokes parameter spectra $\vec{S}(E)$ have been modeled simultaneously in a spectral range of 100 meV around the cavity modes. See SM [33] for further details. Measuring the polarization allows us to discriminate both modes even when they overlap in the total intensity $S_0(E)$. Exemplary spectra are shown in Fig. 2 and in the SM [33].

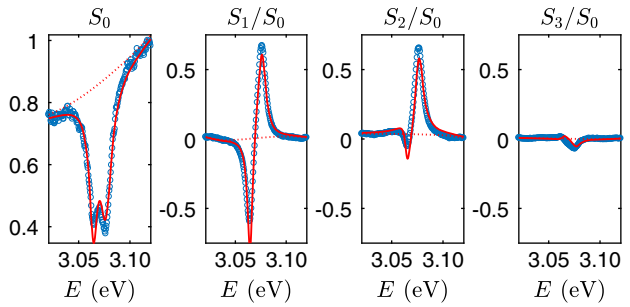

FIG. 2. Representative experimental data (blue dots) and modeling according to Eq. (5) (solid red lines) of normalized Stokes vector spectra $\vec{S}(E)$ at $\vec{k}_\parallel \approx (6.4\,\mu\mathrm{m}^{-1},\ -6.4\,\mu\mathrm{m}^{-1})$, not far from a Voigt point. Dashed red lines represent the baselines. No positive S_3/S_0 occurs.

Results and discussion.—The eigenvalues of the fitted Hamiltonian are shown in Fig. 3 for the entire momentum space ($\vec{k}_\parallel$); their differences [Figs. 3(c) and 3(f)] reveal the locations where degeneracy of either the mode energies ($\Delta E = 0$) or broadenings ($\Delta\Gamma = 0$) occurs. Four Voigt points are found at approximately $(\pm k_x, \pm k_y) \approx (\pm 4\,\mu\mathrm{m}^{-1},\ \pm 8\,\mu\mathrm{m}^{-1})$. These experimental positions agree with theoretical computations [see Figs. A12 (m)–A12(r) in [33]]. Figure 3 is already hinting at the complex-square-root topology: While E_1 and E_2 increase continuously with increasing $|\vec{k}_\parallel|$ in any direction, Γ_1 and Γ_2 are discontinuous along k_y. This is the result of sorting the modes such that $E_1 \le E_2$: the modes are exchanged upon degeneracy ($E_1 = E_2$). Resorting the modes to resolve the discontinuity in $\Gamma_{1,2}$ would result in a discontinuity for $E_{1,2}$ along $\Delta\Gamma = 0$.

To verify the complex-square-root topology of the mode-energy surface, we consider a path in momentum space that encircles an EP. Figure 4 tracks the obtained mode energies for each $\vec{k}_\parallel$ along this path. One round-trip yields a continuous exchange of the two modes; i.e., the energetically higher (and spectrally narrower) mode becomes the energetically lower (and broader) one, and vice versa. This exchange, under quasistatic [42] encirclement, establishes the existence of an EP [7,43,44]. Only encircling the Voigt point twice restores the initial situation. As discussed above, another proof for the existence of EPs is parameter C

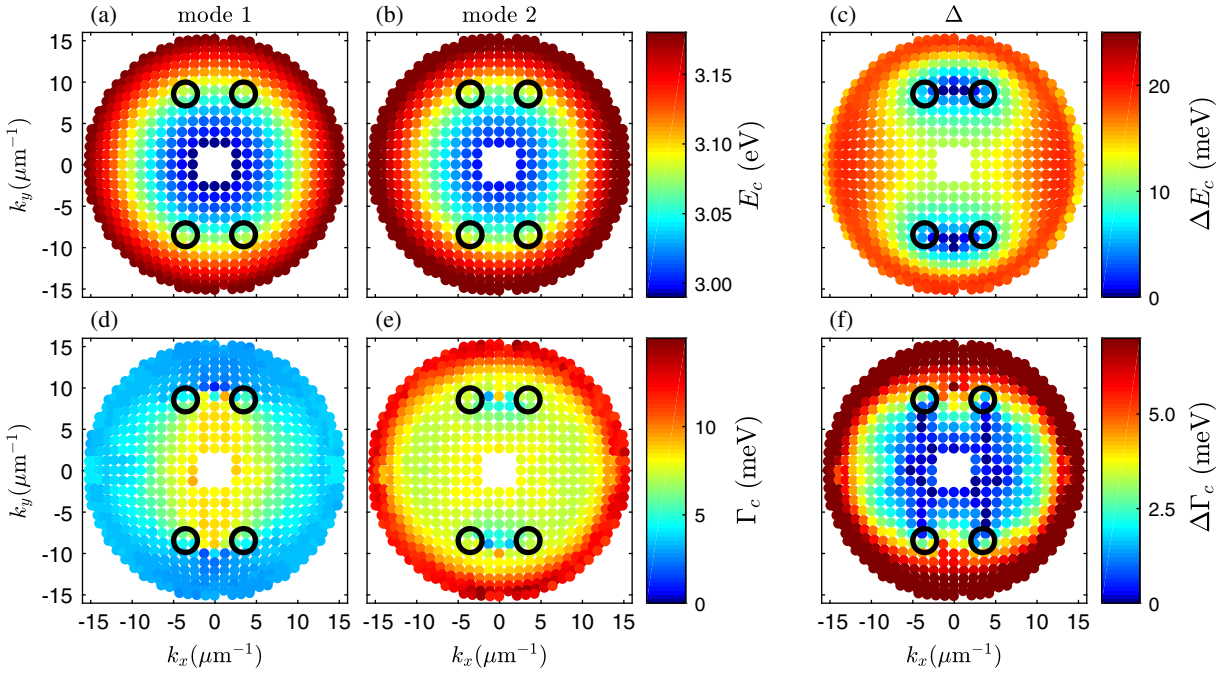

FIG. 3. Complex mode energies $\tilde{E}_{1,2} = E_{1,2} - i\Gamma_{1,2}$ depending on the in-plane wave vector $\vec{k}_\parallel$ from fitting the Hamiltonian. (a),(b) mode energies $E_{1,2}$, (c) their difference $\Delta E = |E_2 - E_1|$. (d),(e) mode broadening $\Gamma_{1,2}$, (f) their differences $\Delta\Gamma = |\Gamma_2 - \Gamma_1|$. The positions of the four Voigt points are marked by black circles. Only here, both ΔE and $\Delta\Gamma$ vanish simultaneously. Modes are sorted such that $E_1 \leq E_2$. For comparison, numerical computations are shown in Figs. A12 (o) and A12(r) in the SM [33].

being nonzero while $E_1 = E_2$. Indeed, we obtain values on the order of -3 meV between the Voigt points (see SM [33]).

Once the EP character of the Voigt points has been proven, we analyze their light polarization. Figure 2 shows that only one circular polarization of the reflected light is detected in the vicinity of a Voigt point [$S_3(E)$] although the linear polarization is still opposite for the two modes [$S_{1,2}(E)$]. Opposite linear polarizations are expected as long as a Voigt point is not exactly met. Figure 5 depicts the polarization patterns in momentum space. It shows the measured Stokes vector values at energies corresponding to the real part of the obtained mode energies [Figs. 3(a) and 3(b)]. The $\vec{k}_\parallel$ dependencies of S_1/S_0 and S_2/S_0 display vortices for the linear polarization: When encircling a pair of Voigt points, the linear polarization changes to the opposite and back. Hence, the pair is a vortex center with winding number one. As expected, S_1/S_0 is discontinuous along k_y when $\Delta E = 0$ [20]. The experimentally determined degree of circular polarization (S_3/S_0), however, hardly exceeds 10%. Slightly higher degrees of circular polarization have been observed from the same sample in photoluminescence and transmission experiments [33,39], which might be related to the discrete $\vec{k}_\parallel$ scan. In principal, a nonsymmetric matrix operator could result in EPs representing elliptic polarization [45]. That could be caused, e.g., by the substrate of the sample. However, numerical computations with proper account of the substrate show that, even in this case, circularly polarized EPs can be expected (see SM [33]). The lack of high degrees of circular polarization in the experiment seems to be a common problem for polarization-resolved experimental studies in chiral photonic structures [46] and reflects the high sensitivity of EPs to perturbations in general [47,48].

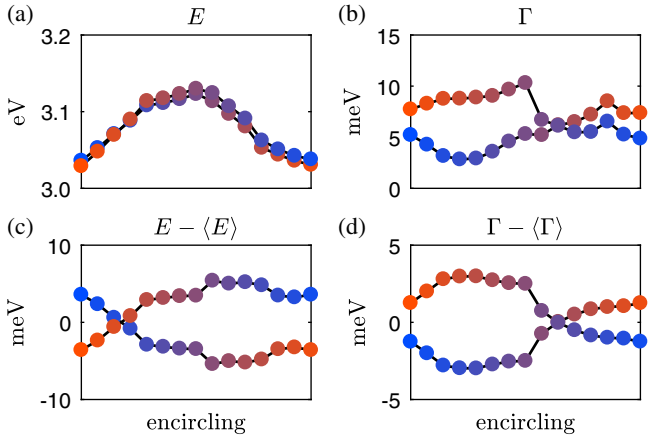

FIG. 4. Clockwise encircling of a Voigt point in $\vec{k}_\parallel$ space along the path shown in Fig. 1(b) with the same color code, starting and ending at $\vec{k}_\parallel \approx (0\ \mu\mathrm{m}^{-1},\ 6\ \mu\mathrm{m}^{-1})$. (a) mode energies degenerate near the fourth point, (b) broadenings near the twelfth. Encircling once flips one mode to the other, encircling twice yields the initial situation (complex-square-root topology). For better visibility, the mean values are subtracted in (c) and (d). See further trajectories in the SM [33].

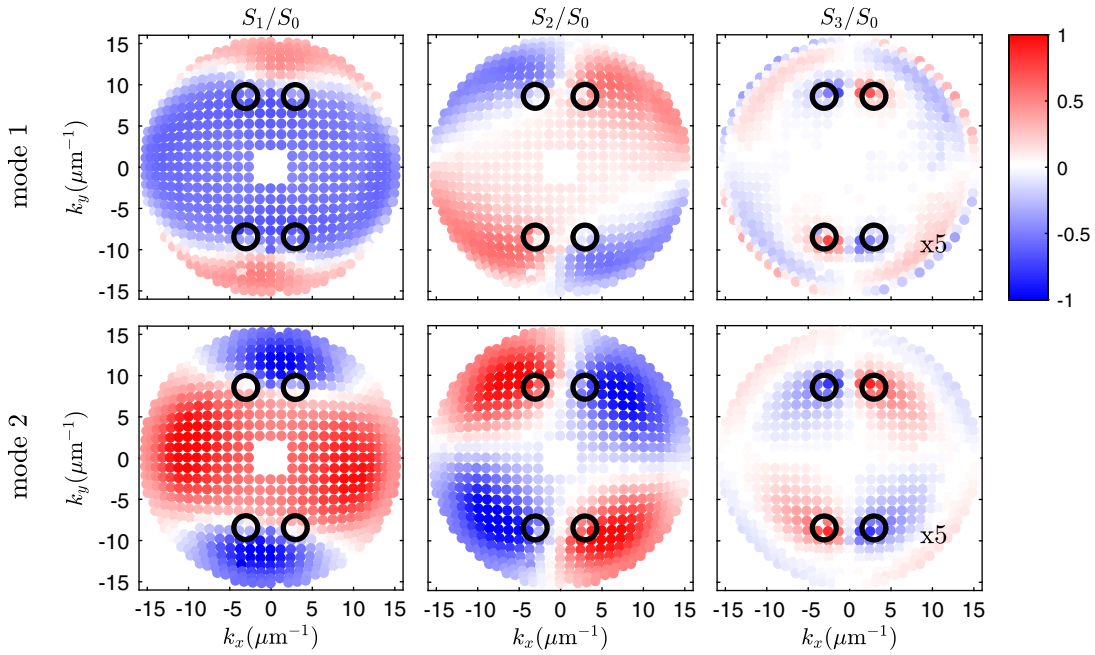

FIG. 5. Measured values of the normalized Stokes vector at the resonance energies obtained from the modeling [Figs. 3(a) and 3(b)]. S_3/S_0 is shown 5 times enhanced. Approximate positions of the Voigt points are marked by black circles where the circular polarization (S_3) of both modes coincides. See SM, Fig. A13(c), for comparison with theoretical expectations [33].

Nonetheless, it is clear from the experimental data that the vicinity of a Voigt point is related to circular polarization.

Conclusion.—In summary, we have implemented a non-Hermitian model system mimicking a biaxial and absorbing crystal by fabricating an entirely dielectric, planar microcavity with an anisotropic cavity layer (*m*-plane oriented ZnO). Fitting an effective Hamiltonian to our polarization-resolved reflectance data allowed us to obtain the optical mode energies and their degeneracies in the two-dimensional momentum space. We have proven the existence of exceptional points by analyzing the complex-square-root topology of the eigenenergy surface. The measured polarization reveals the circularity of these exceptional points and their role as vortex centers for the linear polarization. We suggest the term Voigt points for this special kind of exceptional points. Our findings apply to any planar microcavity with broken cylindrical symmetry and, thus, pave the way to exploiting exceptional points in widespread optoelectronic devices based on planar microcavities such as vertical cavity surface emitting lasers and resonant cavity light emitting diodes.

This work was supported by the Deutsche Forschungsgemeinschaft (DFG, German Research Foundation), Project No. SCHM 2710/3-1 and Project No. 31047526 – Sonderforschungsbereich (SFB) 762, and by Universität Leipzig in the framework of research profile area Complex Matter. S. R. and H.-G. Z. acknowledge support from the Leipzig School of Natural Sciences BuildMoNa. H.-G. Z. was funded by DFG Grant SFB 762, L. T. by DFG Grant Forschergruppe (FOR) 1616 (Project No. SCHM2710/2-2). We also acknowledge the support of the Agence Nationale de la Recherche (ANR) Project "Plug and Bose" (Project No. ANR-16-CE24-0021).

*steffen.richter@eli-beams.eu

[1] L. Lu, J. D. Joannopoulos, and M. Soljačić, Topological photonics, Nat. Photonics **8**, 821 (2014).
[2] A. B. Khanikaev and G. Shvets, Two-dimensional topological photonics, Nat. Photonics **11**, 763 (2017).
[3] J.-X. Zhang, M. C. Rechtsman, and C.-X. Liu, Invited Article: Topological crystalline protection in a photonic system, APL Photonics **1**, 050803 (2016).
[4] X.-C. Sun, C. He, X.-P. Liu, M.-H. Lu, S.-N. Zhu, and Y.-F. Chen, Two-dimensional topological photonic systems, Prog. Quantum Electron. **55**, 52 (2017).
[5] Y. Zhang, A. Chen, W. Liu, C. W. Hsu, B. Wang, F. Guan, X. Liu, L. Shi, L. Lu, and J. Zi, Observation of Polarization Vortices in Momentum Space, Phys. Rev. Lett. **120**, 186103 (2018).
[6] C. Dembowski, H.-D. Gräf, H. L. Harney, A. Heine, W. D. Heiss, H. Rehfeld, and A. Richter, Experimental Observation of the Topological Structure of Exceptional Points, Phys. Rev. Lett. **86**, 787 (2001).
[7] C. Dembowski, B. Dietz, H.-D. Gräf, H. L. Harney, A. Heine, W. D. Heiss, and A. Richter, Encircling an exceptional point, Phys. Rev. E **69**, 056216 (2004).
[8] O. Angelsky, A. Mokhun, I. Mokhun, and M. Soskin, The relationship between topological characteristics of component vortices and polarization singularities, Opt. Commun. **207**, 57 (2002).

[9] D. Leykam, K. Y. Bliokh, C. Huang, Y. D. Chong, and F. Nori, Edge Modes, Degeneracies, and Topological Numbers in Non-Hermitian Systems, Phys. Rev. Lett. **118**, 040401 (2017).

[10] T. Goldzak, A. A. Mailybaev, and N. Moiseyev, Light Stops at Exceptional Points, Phys. Rev. Lett. **120**, 013901 (2018).

[11] T. Gao, E. Estrecho, K. Y. Bliokh, T. C. H. Liew, M. D. Fraser, S. Brodbeck, M. Kamp, C. Schneider, S. Höfling, Y. Yamamoto, F. Nori, Y. S. Kivshar, A. G. Truscott, R. G. Dall, and E. A. Ostrovskaya, Observation of non-Hermitian degeneracies in a chaotic exciton-polariton billiard, Nature (London) **526**, 554 (2015).

[12] T. Gao, G. Li, E. Estrecho, T. C. H. Liew, D. Comber-Todd, A. Nalitov, M. Steger, K. West, L. Pfeiffer, D. W. Snoke, A. V. Kavokin, A. G. Truscott, and E. A. Ostrovskaya, Chiral Modes at Exceptional Points in Exciton-Polariton Quantum Fluids, Phys. Rev. Lett. **120**, 065301 (2018).

[13] J. Zhang, B. Peng, Ş. K. Özdemir, K. Pichler, D. O. Krimer, G. Zhao, F. Nori, Y.-X. Liu, S. Rotter, and L. Yang, A phonon laser operating at an exceptional point, Nat. Photonics **12**, 479 (2018).

[14] Ş. K. Özdemir, S. Rotter, F. Nori, and L. Yang, Parity-time symmetry and exceptional points in photonics, Nat. Mater. **18**, 783 (2019).

[15] B. Zhen, C. W. Hsu, Y. Igarashi, L. Lu, I. Kaminer, A. Pick, S.-L. Chua, J. D. Joannopoulos, and M. Soljačic, Spawning rings of exceptional points out of Dirac cones, Nature (London) **525**, 354 (2015).

[16] B. Peng, Ş. K. Özdemir, M. Liertzer, W. Chen, J. Kramer, H. Yılmaz, J. Wiersig, S. Rotter, and L. Yang, Chiral modes and directional lasing at exceptional points, Proc. Natl. Acad. Sci. U.S.A. **113**, 6845 (2016).

[17] C.-H. Yi, J. Kullig, and J. Wiersig, Pair of Exceptional Points in a Microdisk Cavity under an Extremely Weak Deformation, Phys. Rev. Lett. **120**, 093902 (2018).

[18] T. G. Mackay and A. Lakhtakia, Voigt wave propagation in biaxial composite materials, J. Opt. A **5**, 91 (2003).

[19] C. Sturm and M. Grundmann, Singular optical axes in biaxial crystals and analysis of their spectral dispersion effects in $\beta - Ga_2O_3$, Phys. Rev. A **93**, 053839 (2016).

[20] S. Richter, T. Michalsky, C. Sturm, B. Rosenow, M. Grundmann, and R. Schmidt-Grund, Exceptional points in anisotropic planar microcavities, Phys. Rev. A **95**, 023836 (2017).

[21] M. V. Berry and M. R. Dennis, The optical singularities of birefringent dichroic chiral crystals, Proc. R. Soc. A **459**, 1261 (2003).

[22] H. Lloyd, XXI. On the phænomena presented by light in its passage along the axes of biaxal crystals, Philos. Mag. **2**, 112 (1833).

[23] L. D. Landau and E. M. Lifschitz, Elektrodynamik der Kontinua, in *Elektrodynamik der Kontinua*, edited by G. Heber, Lehrbuch der theoretischen Physik Vol. VIII (Akademie-Verlag, Berlin, 1967).

[24] M. V. Berry and M. R. Jeffrey, Conical diffraction: Hamilton's diabolical point at the heart of crystal optics, in *Progress in Optics*, Vol. 50, edited by E. Wolf (Elsevier, New York, 2008), Chap. 2, p. 13.

[25] M. Grundmann, C. Sturm, C. Kranert, S. Richter, R. Schmidt-Grund, C. Deparis, and J. Zúñiga-Pérez, Optically anisotropic media: New approaches to the dielectric function, singular axes, microcavity modes and Raman scattering intensities, Phys. Status Solidi **11**, 1600295 (2017).

[26] W. Voigt, VII. On the behaviour of pleochroitic crystals along directions in the neighbourhood of an optic axis, Philos. Mag. **4**, 90 (1902).

[27] W. Voigt, Beiträge zur Aufklärung der Eigenschaften pleochroitischer Krystalle, Götting. Nachr. **1**, 48 (1902).

[28] W. D. Heiss and H. L. Harney, The chirality of exceptional points, Eur. Phys. J. D **17**, 149 (2001).

[29] D. Solnyshkov and G. Malpuech, Chirality in photonic systems (Chiralité dans les systèmes photoniques), C.R. Phys. **17**, 920 (2016).

[30] A. A. Soluyanov, D. Gresch, Z. Wang, Q. Wu, M. Troyer, X. Dai, and B. A. Bernevig, Type-II Weyl semimetals, Nature (London) **527**, 495 (2015).

[31] C. Mahaux and H. A. Weidenmüeller, *Shell-Model Approach to Nuclear Reactions* (North-Holland, Amsterdam, 1969).

[32] H. Cao and J. Wiersig, Dielectric microcavities: Model systems for wave chaos and non-Hermitian physics, Rev. Mod. Phys. **87**, 61 (2015).

[33] See Supplemental Material at http://link.aps.org/supplemental/10.1103/PhysRevLett.123.227401 for further experimental and modeling details, additional experimental data, and simulations, which includes Refs [34–37].

[34] H.-G. Zirnstein, G. Refael, and B. Rosenow, Bulk-boundary correspondence for non-Hermitian Hamiltonians via Green functions, arXiv:1901.11241.

[35] W. Suh, Z. Wang, and S. Fan, Temporal coupled-mode theory and the presence of non-orthogonal modes in lossless multimode cavities, IEEE J. Quantum Electron. **40**, 1511 (2004).

[36] S. Fan, W. Suh, and J. D. Joannopoulos, Temporal coupled-mode theory for the Fano resonance in optical resonators, J. Opt. Soc. Am. A **20**, 569 (2003).

[37] L. C. Andreani, *Optical Transitions, Excitons, and Polaritons in Bulk and Low-Dimensional Semiconductor Structures*, edited by E. Burstein and C. Weisbuch, NATO ASI Series Vol. 340 (Springer, New York, 1995).

[38] J. Zúñiga-Pérez, L. Kappei, C. Deparis, F. Reveret, M. Grundmann, E. de Prado, O. Jamadi, J. Leymarie, S. Chenot, and M. Leroux, Homoepitaxial nonpolar (10-10) ZnO/ZnMgO monolithic microcavities: Towards reduced photonic disorder, Appl. Phys. Lett. **108**, 251904 (2016).

[39] S. Richter, Optically anisotropic planar microcavities, Ph. D. thesis, Universität Leipzig 2018, http://nbn-resolving.de/urn:nbn:de:bsz:15-qucosa2-208912.

[40] H. Franke, C. Sturm, R. Schmidt-Grund, G. Wagner, and M. Grundmann, Ballistic propagation of exciton–polariton condensates in a ZnO-based microcavity, New J. Phys. **14**, 013037 (2012).

[41] R. A. Chipman, Polarimetry, in *Handbook of Optics*, edited by M. Bass (McGraw-Hill, New York, 1995), Chap. 22.

[42] For each momentum parameter, the mode energies are determined from separate, stationary experiments with different angles of incidence. We do not perform dynamical encircling of the EP [43,44].

[43] J. Doppler, A. A. Mailybaev, J. Böhm, U. Kuhl, A. Girschik, F. Libisch, T. J. Milburn, P. Rabl, N. Moiseyev, and S. Rotter, Dynamically encircling an exceptional point for asymmetric mode switching, Nature (London) **537**, 76 (2016).

[44] A. U. Hassan, B. Zhen, M. Soljačić, M. Khajavikhan, and D. N. Christodoulides, Dynamically Encircling Exceptional Points: Exact Evolution and Polarization State Conversion, Phys. Rev. Lett. **118**, 093002 (2017).

[45] M. Grundmann, S. Richter, T. Michalsky, C. Sturm, J. Zúñiga-Pérez, and R. Schmidt-Grund, Exceptional points in anisotropic photonic structures: from non-Hermitian physics to possible device applications, Proc. SPIE Int. Soc. Opt. Eng. **10105**, 101050K (2017).

[46] S. Takahashi, Y. Ota, T. Tajiri, J. Tatebayashi, S. Iwamoto, and Y. Arakawa, Circularly polarized vacuum field in three-dimensional chiral photonic crystals probed by quantum dot emission, Phys. Rev. B **96**, 195404 (2017).

[47] J. Wiersig, Sensors operating at exceptional points: General theory, Phys. Rev. A **93**, 033809 (2016).

[48] W. Chen, Ş. K. Özdemir, G. Zhao, J. Wiersig, and L. Yang, Exceptional points enhance sensing in an optical microcavity, Nature (London) **548**, 192 (2017).